Electronic Supplementary Material (ESI) for Polymer Chemistry.

Supplementary Information

Amphiphilic polypyrrole-poly(Schiff base) copolymers with poly(ethylene glycol) side chains: Synthesis, properties and applications

Brenda G. Molina,[1,2] Luminita Cianga,[3] Anca-Dana Bendrea,[3] Ioan Cianga,[3,*] Luis J. del Valle,[1,2] Francesc Estrany, [1,2] Carlos Alemán[1,2,*], Elaine Armelin,[1,2,*]

[1] *Departament d'Enginyeria Química, EEBE, Universitat Politècnica de Catalunya, C/ Eduard Maristany, 10-14, Ed. I.2, 08019, Barcelona, Spain.*

[2] *Barcelona Research Center for Multiscale Science and Engineering, Universitat Politècnica de Catalunya, C/ Eduard Maristany, 10-14, Ed. I.S, 08019, Barcelona, Spain.*

[3] *"Petru Poni" Institute of Macromolecular Chemistry, 41A, Grigore –Ghica Voda Alley, 700487, Iasi, Romania.*

[*] Corresponding author: ioanc@icmpp.ro, carlos.aleman@upc.edu and elaine.armelin@upc.edu

METHODS

Characterization of the macromonomer precursor, bis(pyrrole)benzoic Schiff base, and the macromonomer

^{1}H-NMR and ^{13}C-NMR spectra were recorded at room temperature on a Bruker Avance DRX-400 spectrometer at 400 MHz and 100. 61 MHz, respectively as solutions in DMSO-d_6 or acetone-d_6 and chemical shifts are reported in ppm relative to residual peak of the solvent.

The FTIR spectra were recorded on a Bruker Vertex 70 FTIR spectrometer equipped with a diamond ATR device (Golden Gate, Bruker) in transmission mode, by using KBr pellets.

UV-Vis and fluorescence measurements of samples solutions ($1x10^{-3}$ M) were carried out by using DMSO as solvent on a Specord 200 Analytik Jena spectrophotometer and Perkin Elmer LS 55 apparatus, respectively.

Differential scanning calorimetry (DSC) was performed on a Mettler Toledo DSC822e. Approximately 2-3 mg of samples were tested by applying a heating/cooling rate of 10^{o}C min^{-1} or 2^{o}C min^{-1} from 20^{o}C to 210^{o}C, under nitrogen atmosphere (50 mL min^{-1}).

Thermal stability was analyzed by means of a Mettler Toledo TGA-SDTA851e derivatograph. TG and DTG curves were recorded under nitrogen atmosphere, into a temperature interval of 25^{o}C–700^{o}C, with a heating rate of 10^{o}C min^{-1}. Constant operational parameters were preserved for all the samples, which had the mass ranged between 1.8 and 5.3 mg, so as to obtain comparable data and, moreover, the recordings were repeated for the same heating rate, so as to verify their reproducibility. The curves were processed using the STAR software from Mettler Toledo in order to obtain the thermal and kinetic characteristics.

Characterization of the copolymers. The thickness of the P(Py-*co*-AzbPy-*g*-PEG) films was determined by contact profilometry, using a Dektak 150 stylus profilometer (Veeco, Plainview, NY). Different scratches were intentionally provoked on the films and measured to allow statistical analysis of data. Imaging of the films was conducted using the following optimized settings: tip radius= 2.5 μm; stylus force= 1.5 mg; scan length= 1 μm; and speed= 1.5 nm/s. The thickness was measured using two different items: (i) the vertical distance (VD), which corresponds to the difference between the height polymer and the height of the steel substrate without any average; and (ii) the average step height (ASH), which measures the difference between the average height of the polymer and the average height of the steel substrate.

FTIR spectra were recorded on a Nicolet 6700 spectrophotometer by transmittance. For this purpose, films were scrapped off from the electrode, dried under vacuum and recorded using KBr discs, at a 6 cm^{-1} resolution (64 scans). Raman spectra of the electropolymerized films were obtained through Renishaw InVia confocal Raman microscope, at 532 nm of laser excitation, with an exposure time of 10 s, a laser power of 1% and 4 accumulations.

Scanning electron microscopy (SEM) studies were performed to investigate the effect of the applied synthetic approach on the surface morphology of the films. Dried samples were placed in a Focused Ion Beam Zeiss Neon 40 scanning electron microscope operating at 5 kV, equipped with an EDX spectroscopy system. Topographic images were obtained by atomic force microscopy (AFM) with a Dimension 3100 microscope and a Multimode TM microscope using a NanoScope IV controller (Bruker) under ambient conditions in tapping mode. The root mean square roughness (R_q), which is the average height deviation taken from

the mean data plane, was determined using the statistical application of the NanoScope Analysis software (1.20, Veeco). The scan window size was 5×5 μm^2.

Contact angle measurements were used to study the wettability of the studied films. The sessile water drop method was applied at room temperature and controlled humidity. Images of 5 μL distillated water drops on the nanomembrane surfaces were recorded after stabilization (10 s) with the equipment OCA 20 (DataPhysics Instruments GmbH, Filderstadt). The software SCA20 was used to analyze the images and acquire the contact angle value. Contact angle values were obtained as the average of 10 independent measures for each sample.

The UV-vis spectra of P(Py-*co*-AzbPy-*g*-PEG) and PPy were obtained using an UV-vis-NIR Shimadzu 3600 spectrophotometer equipped with a tungsten halogen visible source, a deuterium arc UV source, a photomultiplier tube UV-vis detector, and an InGaAs photodiode and cooled PbS photocell NIR detectors. Spectra were recorded in the absorbance mode using the integrating sphere accessory (model ISR-3100), the wavelength range was 300-800 nm. Films were deposited onto ITO glass slides for measurements and other uncoated ITO glass sheet was used as reference. Single-scan spectra were recorded at a scan speed of 60 nm/min. Measurements, data collection and data evaluation were controlled by the software UVProbe version 2.31.

The electroactivity and electrostability were studied by cyclic voltammetry (CV) using an acetonitrile solution containing 0.1 M of $LiClO_4$. The initial and final potentials were –0.50 V, and the reversal potential was 2.00 V. A scan rate of 50 mV/s was used in all cases. The electroactivity and electrostability were determined through direct measure of the anodic and cathodic areas in the control voltammograms, using the GPES software.

Protein adsorption. The ability of the P(Py-*co*-AzbPy-*g*-PEG) films to interact with different types of proteins was examined through adsorption assays using albumin (BSA) and Lysozyme (Lyz) proteins. For this purpose, steel sheets covered by P(Py-*co*-AzbPy-*g*-PEG) (θ= 1000 s) and PPy (θ= 300 s), as well as steel sheets as bare substrates were immersed in 500 µL of BSA and Lyz aqueous solutions (c= of 1%), at 37 °C with moderate stirring. After 48 hours of immersion, samples were washed with deionized water and dried at room conditions. Once every electrode was completely dry, 300 µL of extraction buffer (Tris 0.625M, SDS 2%, BME 5%) were added and incubated for one hour. Then, the protein concentrations were determined by the colorimetric Ninhydrin reaction. The solutions were prepared by mixing the same amount of the proteins extracted for the different surfaces with Ninhydrin. Later the samples were heated at 95 °C for 10 min and the absorbance at 570 nm was measured in a microplate reader (EZ Read 400– Biochrom, UK) with ADAP 2.0 Plus Data Analysis Software. In order to ascertain the concentration of protein adsorbed onto the surfaces, it was necessary to make a calibration graph (*i.e.* protein concentration versus the absorbance). This was constructed by above described procedure, but replacing the proteins extracted from polymer surfaces with solutions having known concentrations of Lyz and BSA.

Cytotoxicity. Cellular assays were performed using COS-1 and Vero cell lines, which selected due to their fast growth. Cells were cultured in DMEM high glucose supplemented with 10% FBS, penicillin (100 units/mL), and streptomycin (100 µg/mL). The cultures were maintained in a humidified incubator with an atmosphere of 5% CO_2 and 95% O_2 at 37ºC.

Culture media were changed every two days. When the cells reached 80-90% confluence, they were detached using 1-2 mL of trypsin (0.25% trypsin/EDTA) for 5 min at 37 °C. Finally, cells were re-suspended in 5 mL of fresh medium and their concentration was determined by counting with a Neubauer camera using 0.4% trypan blue as a vital dye.

P(Py-*co*-AzbPy-*g*-PEG) and PPy deposited onto steel AISI 316 sheets of 0.5 cm^2 were placed in plates of 24 wells and sterilized using UV irradiation for 15 min in a laminar flux cabinet. Controls were simultaneously performed by culturing cells onto the surface of steel plates. For cytotoxicity assays, an aliquot of 50 μL containing 5×10^4 cells was deposited on the film of each well. Then, attachment of cells to the film surface was promoted by incubating under culture conditions for 30 min. Finally, 500 μL of the culture medium were added to each well. After 72 h, all cells in the well were quantified to evaluate the cytotoxicity of the materials.

Cellular viability was evaluated by the colorimetric MTT [3-(4,5-dimethylthiazol-2-yl)-2,5-diphenyltetrazolium bromide] assay.[1] This assay measures the ability of the mitochondrial dehydrogenase enzyme of viable cells to cleave the tetrazolium rings of the MTT and form formazan crystals, which are impermeable to cell membranes and, therefore, are accumulated in healthy cells. This process is detected by a color change: the characteristic pale yellow of MTT transforms into the dark-blue of formazan crystals. Specifically, 50 mL of MTT solution (5 mg/mL in PBS) were added to each well. After 3 h of incubation, samples were washed twice with PBS and stored in clean wells. In order to dissolve formazan crystals, 1 mL of DMSO/methanol/water (70/20/10 % v/v) was added. Finally, the absorbance was measured in a plate reader at 570 mm. The viability results, derived from the average of three replicates

(n= 3) for each independent experiment, were normalized to steel substrate as control, for relative percentages.

Antibacterial activity. The antimicrobial effect of steel substrate, AzbPy-*g*-PEG macromonomer, PPy homopolymer and P(Py-*co*-AzbPy-*g*-PEG) graft copolymer (generated at θ= 1000s) was evaluated using Gram-negative and Gram-positive bacteria, *Escherichia coli* (*E. coli*) and *Staphylococcus aureus* (*S. aureus*) respectively. Five hundred colony forming units (CFU) were seeded in 12 mL of broth culture and then 0.5 mL were added to each Eppendorf tube that contains steel sheets, PPy and P(Py-*co*-AzbPy-*g*-PEG) films. For the macromonomer, AzbPy-*g*-PEG, 1.5 mg was solubilized in 150 µL of water and then an aliquot of 30 µL of the solution was seed with the bacteria. All the samples and the control were vortexed for 1 min, and incubated at 37ºC with agitation at 80 rpm for 24 hours. UV absorbance was measured at λ595 nm to starting and finishing the experiment. The bacteria number was the results of the second reading minus the first one.

Statistical analyses were performed with a confidence level of 95% ($p<0.05$) using Student's T-test.

Electrochemical detection of serotonin neurotransmitter. Due to its high sensitivity for quantitative analysis, differential pulse voltammetry (DPV) was applied as a methodology for the electrochemical detection of serotonin. The assays were carried out in a tree electrode cell, as that described in the main text, changing the stainless steel WE by a glassy carbon electrode (3.14×10^{-2} cm^2 of surface area). The potential range applied was from -0.3V to +0.7 V, with 80 mV as modulation amplitude and a scan increment of 2 mV. The modulation and

interval time were 0.05 and 40 s, respectively. The DPV signal corresponding to electrochemical oxidation of serotonin was recorded in PBS (pH 7.4) solutions with serotonin concentrations ranging from 0 μM to 20 μM.

RESULTS AND DISCUSSION

Structural characterization, photophysical and thermal properties of AzbPy-g-PEG macromonomer and its precursor AzbPyBA

^{13}C-NMR spectra support the results obtained by FTIR and ^{1}H-NMR spectroscopies.

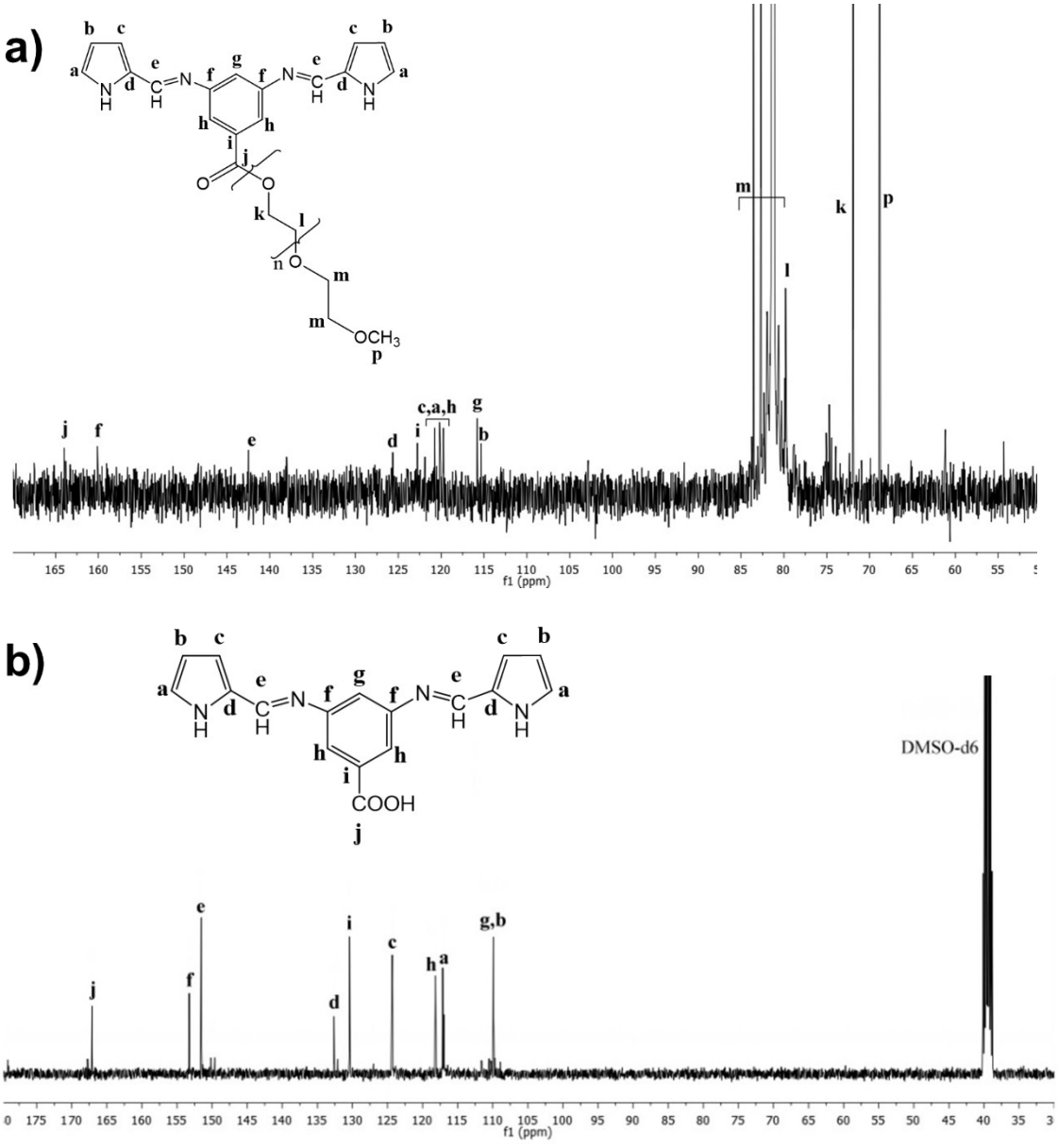

Figure S1. ^{13}C-RMN spectra of (a) AzbPy-*g*-PEG monomer and (b) AzbPyBA precursor in DMSO-*d6*.

Concerning UV-vis absorption properties, Table 1 (main text) indicates that λ_{max} and E_g do not suffer any change when the end-heterocycle groups changes from thiophene to pyrrole. AzbPyBA exhibits strong absorption capacity in comparison with AzbT[2] and other triphenylamine (TPA)-containing bis(pyrrole)- azomethines.[3] Thus, the molar extinction coefficient (**ε**) of AzbPyBA is 30 and 8 times greater than that of AzbT and TPA-containing bis(pyrrole)-azomethines,[3] respectively. These results have been attributed to the different behavior of the moieties enclosed between the azomethine linkages. While TPA is a well-recognized electron-donor, the presence of the electron withdrawing carboxyl group in AzbPyBA could be responsible for the registered difference. Regarding the fluorescence study, both the curve shape and the $\boldsymbol{\lambda_{max}}$ value changed by replacing thiophene by pyrrole. While the fluorescence curve of AzbT is bimodal[2], AzbPyBA shows a non-symmetric, monomodal shape (Figure S2) and the value of $\boldsymbol{\lambda_{max}}$ is blue shifted (Table 1).

The most important differences in the photophysical properties were observed when PEG was grafted in the structure of (bis)pyrrole azomethine molecule. By comparing with its precursor (AzbPyBA), AzbPy-*g*-PEG macromonomer shows red shifted values for both UV-vis and fluorescence $\boldsymbol{\lambda_{max}}$ values, while keeps a high **ε** value and the optical band gap decreases to 2.48 eV. All of these variations are due to the electron-donor character of the PEG side chain.

It is also important to note the appearance in the UV-vis spectrum of AzbPy-*g*-PEG of an additional absorption band centered at 458 nm. The appearance of this band has been attributed to the formation of micellar “core-shell” type nano-objects by self-assembling in PEG-selective DMSO solvent. Indeed, the introduction of PEG chains in AzbPy-*g*-PEG enhances both the stiff asymmetry and the amphiphilic character, enabling this association.

Due to spatial constraint of the formed entities, the molecules inside can come in a closer proximity, allowing for a more efficient "self-recognition" through hydrogen bonds and having an extended conjugation in a similar manner as it was previously reported for (bis)pyrrole azomethines in solid state.[4] The extended conjugation of such oligomer-like structures could be responsible for the presence of absorption peak at 458 nm in the UV-vis curve of AzbPy-*g*-PEG. In fact, it was already demonstrated that the self-assembly by complementary hydrogen bonds is feasible for (bis)pyrrole azomethines in solution.[5]

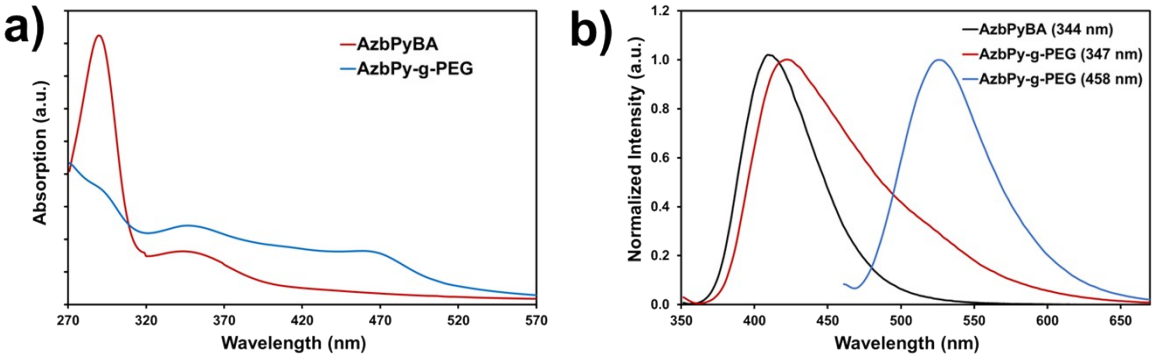

Figure S2. (a) UV-vis spectra of AzbPyBA (red curve) and AzbPy-*g*-PEG (blue curve) in DMSO; and (b) fluorescence spectra of AzbPyBA (black curve, λ_{exc}=344nm), AzbPy-*g*-PEG (red curve, λ_{exc}=347nm) and AzbPy-*g*-PEG (blue curve, λ_{exc}=458nm) in DMSO.

The thermal behavior of AzbPyBA and AzbPy-*g*-PEG was assessed by TGA and DSC (Figure S3). DSC experiments were performed in the temperature interval below the degradation temperature (*i.e.* 209°C for AzbPyBA and 354°C for AzbPy-*g*-PEG). Figure S3a displays the first heating run for AzbPyBA, which was conducted at a heating rate of 10 °C/min. The observed thermal phenomena can be described as follows: (i) a very shallow transition, which has been attributed to the glass transition temperature, was detected at around 45°C; (ii)- around 118 and 126°C two glass transition-like peaks can be seen; and (iii)

an exothermic transition starts at around 175 ºC, having a peak at 208 ºC that is immediately followed by an endothermal peak at 210 ºC. It was assumed that in the 175ºC-210ºC range three thermal phenomena could take place: cold crystallization, melting and starting of the degradation. In the cooling run, a large exothermic peak in the range 210 ºC-150 ºC was registered with peak centered at 201 ºC. This exothermic response could be assigned to crystallization but also to other thermal modifications that can take place due to the compositionally and geometrically sophisticated structure of this compound. In the second heating run only the first shallow transition and the beginning of exoterm are visible. In order to make clearer these assumptions, we performed a second DSC experiment, (Figure S3b), the sample was run in a cycle heating-cooling at the scan rate of 10 ºC/min in the range 20-150 ºC (in order to do not interfere with the transitions at 118ºC and 126 ºC) and, then, the sample was heated at a scan rate of 2 ºC/min in the second heating step. The second heating curve presents a sharp exothermic peak centered at 207 ºC due to the cold crystallization, which is typical for glass-forming Schiff-bases molecules and is usually preceded by a glass transition and followed by melting.[6,7] In the investigated temperature range, AzbPy-*g*-PEG shows the melting temperature usually observed for PEG homopolymers and also its typical crystallization temperature in the cooling cycle (Figure S3c).

TGA analyses indicate that AzbPy-*g*-PEG precursor molecule, AzbPyBA, starts to decompose at around 220 ºC, whereas the macromonomer starts at ~354ºC ($T_{d,0}$) with maximum decomposition temperature at 405ºC ($T_{d,max}$) (Figure S3d). The chair yield percentage at 900ºC was similar for both compounds (Table 1).

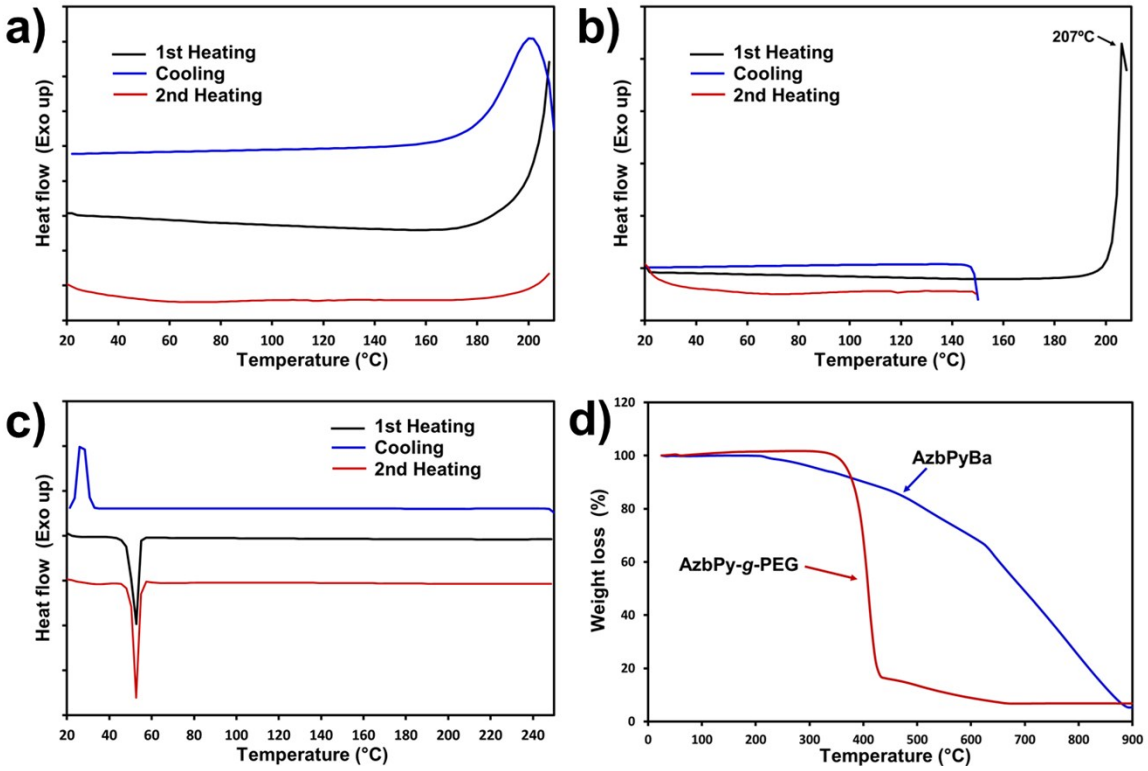

Figure S3. DSC thermograms for: (a) AzbPyBA with heating and cooling run at a scan rate of 10 ºC/min; (b) AzbPyBA with the second heating run at a scan rate of 2 ºC/min; (c) AzbPy-*g*-PEG macromonomer with heating and cooling run at a scan rate of 20 ºC/min. (d) Thermogravimetric curves for the AzbPyBA precursor and the AzbPy-*g*-PEG macromonomer at 10 °C/min in nitrogen atmosphere.

Table S1. FTIR assignments for the main vibrational bands of PPy and P(Py-*co*-AzbPy-*g*-PEG).

Vibrational wavenumbers (cm^{-1})				Assignments
Py	PPy	P(Py-*co*-AzbPy-*g*-PEG		
		Pyrrole units	*PEG side chain*	
3391				N-H stretching vibrations
3125				C-H$^{\alpha}$ stretch (Py ring)
3102				C-H$^{\beta}$ stretch (Py ring)
864				C-H$^{\beta}$ out-of-plane deformation
720				C-H$^{\alpha}$ out-of-plane deformation
	3431			N-H stretching vibrations
	1628			C=N Schiff base vibrations
	1526			C=C stretching of Py ring
	1429			C-N stretching
	1396			C-N stretching
	1146			C-H in-plane vibration
	1114			C-H in-plane vibration
	1082			C-H in-plane vibration
	1021			N-H in plan deformation
	888			C-H out-of-plane deformation
	776			C-H out-of-plane ring deformation
	627			C-C out-of-plane ring deformation or C-H rocking
		3140-3648		N-H stretching vibrations
		1625		C=C stretching of pyrrole ring / Benzene group
		1347		C-N stretching vibration
			2885	C-H symmetric stretching
			1716	C=O group from ester linkage
			1470	CH_2 scissoring vibrations
			1281	C-O-C ether group
			1239	C-O-C ether group
			1110	C-O-C ether group

Table S2. Maximum absorption and optical band gap for PPy and P(Py-*co*-AzbPy-*g*-PEG).

Sample	**Polymerization time (s)**	**λ_{max} [a] (nm)**	**λ_{min} [b] (nm)**	**E_g [c] (eV)**
PPy homopolymer	300	381, 451	551	2.25
P(Py-*co*-AzbPy-*g*-PEG)	300	369, 450	539	2.30
P(Py-*co*-AzbPy-*g*-PEG)	500	370, 449	547	2.27
P(Py-*co*-AzbPy-*g*-PEG)	1000	369, 451	544	2.28

[a] Maximum absorption bands obtained by UV-visible, in solid state. [b] Minima absorption band obtained by the intersection of the line of best fit to the lower absorption band and the tangent to the minimum absorption wavelength showed at Figure 5b (main text). [c] E_g calculated as: $E_g = 1.24 \times 10^3/\lambda_{min}$.

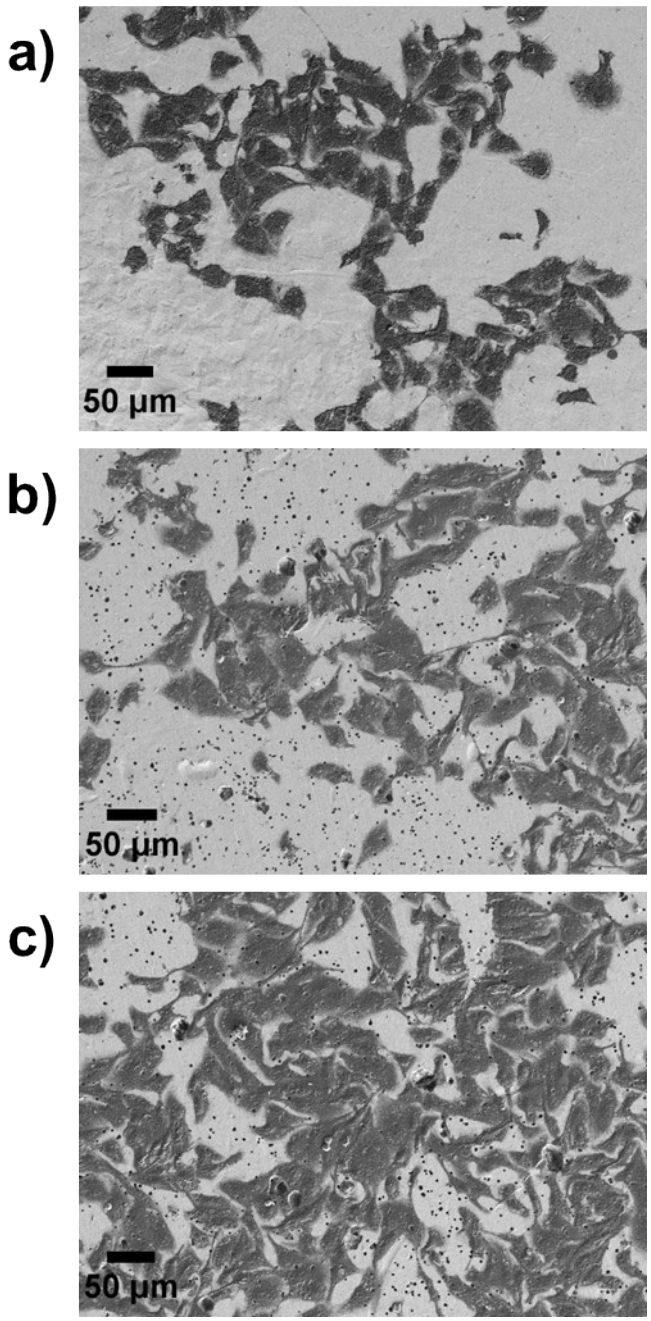

Figure S4. Cos-1 cell after 7 days cultured: a) steel; b) PPy homopolymer; and c) P(Py-*co*-AzbPy-*g*-PEG) copolymer.

References

1 M. N. Patel and S. H. Patil, *J. Macromol. Sci. Part A - Chem.*, 1982, **17**, 675–687.

2 M. M. Pérez-Madrigal, L. Cianga, L. J. del Valle, I. Cianga and C. Alemán, *Polym. Chem.*, 2015, **6**, 4319–4335.

3 Y. Li, Y. Zhang, H. Niu, C. Wang, C. Qin, X. Bai and W. Wang, *New J. Chem.*, 2016, **40**, 5245–5254.

4 O. Q. Munro and G. L. Camp, *Acta Crystallogr. Sect. C Cryst. Struct. Commun.*, 2003, **59**, o672–o675.

5 O. Q. Munro, S. D. Strydom and C. D. Grimmer, *New J. Chem.*, 2004, **28**, 34-42.

6 M. L. Petrus, R. K. M. Bouwer, U. Lafont, S. Athanasopoulos, N. C. Greenham and T. J. Dingemans, *J. Mater. Chem. A*, 2014, **2**, 9474–9477.

7 D. Sek, M. Grucela-Zajac, M. Krompiec, H. Janeczek and E. Schab-Balcerzak, *Opt. Mater. (Amst).*, 2012, **34**, 1333–1346.